Supporting Information

A Coupled Electrocatalytic System with Reduced Energy Input for CO_2 Reduction and Biomass Valorization

Shao-Qing Liu,[ab] Min-Rui Gao,[b] Shuwen Wu,[b] Renfei Feng,[c] Yicheng Wang,[b] Linfang Cui,[a] Ying Guo,[a] Xian-Zhu Fu[a] and Jing-Li Luo*[ab]

[a] Shenzhen Key Laboratory of Energy Electrocatalytic Materials, Shenzhen Key Laboratory of Polymer Science and Technology, Guangdong Research Centre for Interfacial Engineering of Functional Materials, College of Materials Science and Engineering, Shenzhen University, Shenzhen 518060, China.

[b] Department of Chemical and Materials Engineering, University of Alberta, Edmonton, Alberta, T6G 1H9, Canada

[c] Canadian Light Source Inc. Saskatoon, Saskatchewan S7N 0X4, Canada

Experimental Section

Synthesis of cathode Cu_1Bi catalysts for eCO_2RR.

The Cu-BiOON precursor was synthesized by a hydrothermal method. Typically, 2 mmol $Bi(NO_3)_2{\cdot}5H_2O$ and 1.37 mmol CTAB were mixed in 60 ml DI water. After vigorous stirring for 30 min, 0, 0.1, 0.2, or 0.4 mmol $Cu(acac)_2$ was added and continuously stirred for another 30 min. A homogeneous solution of urea (40 ml, 1.25 M) in ethanol was prepared in another beaker by an ultrasonic homogenizer. After cooling, the urea-ethanol solution was quickly added to the above Bi and Cu-containing solution and stirred for 30 min to form a homogeneous solution. This mixture was then transferred into a water bath and kept at 90 °C for 4 h. After cooling to room temperature, the products were collected by centrifugation, washed with ethanol and DI water, and vacuum dried at 40 °C overnight.

The Cu_1Bi catalyst was prepared by *in situ* electrochemical reduction. Typically, 10 mg Cu-BiOON and 10 mg Vulcan XC-72 carbon black were well dispersed in 1 ml solution containing 750 μl isopropanol, 230 μl DI water, and 20 μl Nafion (5 wt%) by ultrasonication for 1 h. Then, 400 μl of the above ink was loaded on a gas diffusion electrode (1 × 1cm^2, Sigracet 22 BB) and reduced at –100 mA cm^{-2} for 30 min in a standard three-electrode flow cell fed with CO_2, with 1 M KOH as electrolyte. The obtained electrode was used directly for later eCO_2RR. With increasing the feeding amount of $Cu(acac)_2$ from 0 to 0.4 mmol during the hydrothermal process, the catalysts with different Cu contents were obtained and denoted as Bi, Cu_1Bi (L), Cu_1Bi, and Cu_1Bi (H).

Synthesis of anode NiCoLDH/NF catalysts for HMFOR.

Nickel foam ($2 \times 2cm^2$) was firstly washed with acetone, 1 M HCl, and DI water under sonication for 10 min, respectively. 0.8 mmol $CoCl_2 \cdot 6H_2O$, 0.2 mmol $NiCl_2 \cdot 6H_2O$, and 1 mmol terephthalic acid were dissolved in a mixture solution containing 10.5 ml N,N-Dimethylformamide, 0.75 ml DI water, and 0.75 ml ethanol. Then, the washed nickel foam was immersed into the solution and transferred to a Teflon-lined autoclave. After heat treatment at 125 °C for 12 h, the NiCoMOF-loaded Ni foam (NiCoMOF/NF) was cleaned with water and ethanol. The NiCoLDH/NF catalyst was obtained by electrochemical CV treatment of NiCo MOF/NF between –0.3 V and 0.65 V *vs*. Hg/HgO with the scan rate of 50 mV s^{-1} for 20 cycles in 1.0 M KOH.

Characterization

Power X-ray diffraction was performed on a Rigaku Ultima IV diffractometer with Cu radiation (40 kV, 44 mA). XPS was conducted on a Kratos AXIS Ultra spectrometer. SEM images were carried out on a Zeiss Sigma field emission scanning electron microscope. High-resolution TEM images were acquired by a JEOL JEM-ARM200CF transmission electron microscope with a field emission gun operated at 200 kV. XAS measurements were performed at the beamline VESPERS at Canadian Light Source. *Ex situ* Cu K-edge XANES and EXAFS data were collected in fluorescence mode. *In situ* Bi L-edge XANES was carried out using a custom-made H-cell with catalysts-loaded carbon paper as the working electrode, a carbon rod as the counter electrode, and a saturated calomel electrode (SCE) as the reference electrode. During the measurements, CO_2 continued to flow into the electrolyte. All the collected XAS data were processed using the ATHENA software. An inductively coupled plasma-optical emission spectrometer (ICP-OES) was measured on Thermo iCAP6300 Duo.

Electrochemical measurements of cathodic eCO_2RR in a flow cell

All electrochemical CO_2 reduction measurements were conducted at room temperature in a typical three-electrode flow cell using catalysts-coated gas-diffusion electrodes (GDEs) as the working electrode, platinum foil as the counter electrode, and Hg/HgO as the reference electrode. The cathode and anode chambers were separated by an anion exchange membrane (AEM, Fumatech FAA-PK-130). 1 M KOH was used as both catholyte and anolyte, circulated using peristaltic pumps at a flow rate of 10 ml min^{-1}. The CO_2 gas was continuously supplied at 20 ml min^{-1} by a flowmeter. A Gamry Interface 1000 potentiostat was employed for recording the electrochemical responses, and the potentials were *iR*-compensated using the Current Interrupt mode. Double-layer capacitance (C_{dl}) was measured by performing cyclic voltammetry (CV) in a non-Faradaic region to evaluate the electrochemical surface area (ECSA). All the electrode potentials were converted to the reversible hydrogen electrode (RHE) using the expression E (RHE) = E (Hg/HgO) + 0.098 + pH × 0.0592.

Electrochemical measurements of anodic HMFOR

All the electrochemical measurements were conducted in a three-electrode H-cell using the as-synthesized NiCoLDH/NF (0.5 × 1cm^2) as the working electrode, carbon rod as the counter electrode, and Hg/HgO as the reference electrode. 1 M KOH with or without the presence of 10 mM HMF was used as the electrolyte. The linear sweep voltammetry curves were recorded with a scan rate of 5 mV s^{-1}, and the potentials were *iR*-compensated using the Current Interrupt mode. The stability towards HMFOR was evaluated by chronoamperometry at 0.41 V vs Hg/HgO in 1 M KOH with 10 mM HMF for five successive runs.

Electrochemical measurements of coupled eCO_2RR-HMFOR electrolysis in MEA system

A commercial MEA electrolyzer (4cm^2) was used to evaluate the coupled eCO_2RR-HMFOR electrolysis. The cathode (Cu_1Bi-loaded GDE) and anode (NiCoLDH/NF) were separated by an AEM (Sustainion X37-50 Grade RT, Dioxide Materials). Upon completion of the electrolyzer assembly, the humidified CO_2 was fed into the cathode with a flow rate of 50 mL min^{-1}, while the anolyte (1 M KOH with the presence of 100 mM HMF) flowed through the anode with a flow rate of 15 mL min^{-1}. The formate produced from eCO_2RR was collected from the anodic and cathodic streams simultaneously, while the FDCA produced from HMFOR was collected from the anodic stream.

eCO_2RR products analysis

The gas products were analyzed by gas chromatograph (GC, Agilent 6890N) equipped with a thermal conductivity detector (TCD) and flame ionization detector (FID). The Faradaic efficiency for gas products (FE_g) was calculated as follows. The volume flow of gas product from the cathode was calculated using the fraction of the gas product (V_g) measured by GC and outlet gas flow rate(u) measured at room temperature (T) and ambient pressure (P). With the number of electrons transferred to produce gas product (n_g) and Faraday constant (F), the partial current for gas product i_g was calculated. Comparing the partial current to the total current i_{total} yielded the FE_g:

$$FE_g = \frac{i_g}{i_{total}} \times 100\% = \frac{F \times n_g \times P \times V_g \times u}{R \times T \times i_{total}} \times 100\%$$

Liquid products were analyzed by an ionic chromatograph (IC) and quantified according to the calibration curve. The Faradaic efficiency for formate ($FE_{formate}$) was calculated as follows. The formate concentration (c) was determined from the IC. With the number of electrons transferred to produce formate (n_l), Faraday constant (F), and the electrolyte volume in the cell (V), the partial

charge to produce formate (Q_l) was calculated. Comparing the partial charge to the total charge passed (Q_{total}) yielded the Faradaic efficiency of formate:

$$FE_{formate} = \frac{Q_l}{Q_{total}} \times 100\% = \frac{n_l \times c \times V \times F}{Q_{total}} \times 100\%$$

With the total current density (j_{total}), the partial current density of formate was calculated using the following equation:

$$j_{formate} = FE_{formate} \times j_{total}$$

The formate production rate was calculated using the following equation:

$$Production\ rate = \frac{Q_{total} \times FE_{formte}}{F \times 2 \times t \times S}$$

Where t is the reaction time and S is the geometric area of the working electrode.

The cathodic half-cell energy conversion efficiencies (EE) were calculated as follows:

$$EE = \frac{(1.23 - E_{formate}) \times FE_{formate}}{1.23 - E}$$

Where $E_{formate}$ is the thermodynamic potential of eCO$_2$RR to formate, E is the applied potential *vs* RHE.

HMFOR products analysis

To identify and measure the amount of HMF and its oxidation products, high-performance liquid chromatography (HPLC) on Shimazdu LC-20 was used. The HPLC system was equipped with a DAD detector column (5 um C18, 4.6 × 150 mm), and a UV–vis detector was set at λ =245 nm.

The column temperature was maintained at 25 °C. An eluent comprising 70% 5 mM ammonium formate aqueous solution and 30% methanol was used. A 30 uL sample of the electrolyte solution was taken and mixed with 1470 uL of deionized water. An injection volume of 1 mL was applied, and the identification and quantification of reactants and oxidation products were determined using calibration curves of commercially available compounds with known concentrations.

The FE of FDCA (FE_{FDCA}) was calculated according to the following equation:

$$FE_{FDCA} = \frac{m_{FDCA} \times n \times F}{Q_{total}} \times 100\%$$

Where m_{FDCA} is the mole of FDCA produced, n is the number of electrons transferred to produce FDCA, F is the Faraday constant, and Q_{total} is the total charge passed.

Density functional theory (DFT) calculation

The Vienna Ab Initio Package (VASP)[1, 2] was employed to perform all the density functional theory (DFT) calculations within the generalized gradient approximation (GGA) using the PBE[3] formulation. The projected augmented wave (PAW) potentials[4, 5] were chosen to describe the ionic cores and valence electrons were taken into account using a plane wave basis set with a kinetic energy cutoff of 400 eV. Partial occupancies of the Kohn−Sham orbitals were allowed using the Gaussian smearing method and a width of 0.05 eV. The electronic energy was considered self-consistent when the energy change was smaller than 10−5 eV. A geometry optimization was considered convergent when the force change was smaller than 0.02 eV/Å. Grimme's DFT-D3 methodology[6] was used to describe the dispersion interactions.

The equilibrium lattice constants of hexagonal Bi unit cell were optimized, when using a 7×7×3 Monkhorst-Pack k-point grid for Brillouin zone sampling, to be a=4.570 Å, c=11.715 Å. It was

then used to construct a Bi(012) surface model (model 1) with p(3×1) periodicity in the x and y directions and 3 atomic layers in the z direction separated by a vacuum layer in the depth of 15 Å in order to separate the surface slab from its periodic duplicates. Model 1 comprised of 54 Bi atoms, Model 2 was built by replacing one Bi on the outmost layer of model 1 with one Cu atom. During structural optimizations, the gamma point in the Brillouin zone was used for k-point sampling, and the bottom two atomic layers were fixed while the top one was allowed to relax.

The adsorption energy (E_{ads}) of adsorbate A was defined as

$$E_{ads} = E_{A/surf} - E_{surf} - E_{A(g)}$$

where $E_{A/surf}$, E_{surf} and $E_{A(g)}$ are the energy of adsorbate A adsorbed on the surface, the energy of clean surface, and the energy of isolated A molecule in a cubic periodic box with a side length of 20 Å and a 1×1×1 Monkhorst-Pack k-point grid for Brillouin zone sampling, respectively.

The free energy of a gas phase molecule or an adsorbate on the surface was calculated by the equation G = E + ZPE − TS, where E is the total energy, ZPE is the zero-point energy, T is the temperature in kelvin (298.15 K is set here), and S is the entropy.

Technoeconomic analysis

To evaluate the economic feasibility of the eCO_2RR-to-formate coupled HMFOR-to-FDCA system, a simplified preliminary technoeconomic analysis was performed according to a model from previous reports.[7, 8] The processing capacity of the plant is 200 tonne of CO_2 per day. The prices of input chemicals and products are listed in Table S2. In this model, the costs under consideration included the electricity, separation, catalyst, membrane, electrolyzer, installation, input chemicals, maintenance, operation, and balance of plant. Below is the list of assumptions made for the calculations.

1. The capital costs of electrolyzer is sensitive to the operating current density, we assume a cost of \$10,000 per m^2 of electrolyzer. The total catalyst and membrane cost are 5 % of the electrolyzer cost.

2. The electricity price is assumed to be 0.1 \$/kWh.

3. The balance of plant is 20 % of the total capital costs.

4. Both the operation and maintenance costs are 10 % of the total capital costs.

5. The installation cost is 35 % of the total capital costs.

6. The capacity factor is assumed to be 0.8.

7. The lifetime of plant is assumed to be 10 years.

The calculation process.

1. Electricity costs

The total charge required to convert 200 tonne of CO_2 is:

$$Q = \frac{Mass\ of\ CO_2\ converted \times F \times N}{Molar\ mass\ of\ CO_2 \times Faradaic\ efficiency}$$

Where Q is the total charge, F is the Faraday's constant and N takes the value 2 since CO_2RR-to-formic acid is a two-electron transfer process.

The corresponding current required to sustain this process can be calculated as follows, with a capacity factor of 0.8.

$$I = \frac{Q}{Time\ in\ a\ day \times Capacity\ factor}$$

Where I is the current.

The power required to sustain this process can be calculated as follows:

$$P = \frac{U \times I}{1000}(kW)$$

Where U is the operating cell voltage and P is the power.

The energy used per day can be calculated as follows:

$$Energy\ used\ per\ day = P \times Time\ in\ a\ day \times Capacity\ factor$$

The electricity cost per day, normalized by the mass of formic acid produced can be calculated:

$$Electricity\ cost\ per\ day = \frac{Energy\ used\ per\ day \times Electricity\ price}{Mass\ of\ formic\ acid\ produced}$$

2. Separation costs

The separation costs are 50 % of the electricity costs.

$$Seperation\ costs = Electricity\ costs \times 50\%$$

3. Capital costs

The area of electrolyser is calculated as follows:

$$Area\ of\ electrolyser = \frac{I}{J}$$

Where J is the operating current density.

The electrolyser cost can be calculated based on the assumption of \$10,000 per m^2.

$$Cost\ of\ electrolyser = Area\ of\ electrolyser \times 10000$$

The total catalyst and membrane costs are assumed to be 5 % of the electrolyser cost and is calculated as follows:

$$Cost\ of\ catalyst\ and\ membrane = Cost\ of\ electrolyser \times 5\%$$

Finally, the capital costs can be calculated:

$$Capital\ costs = \frac{Cost\ of\ electrolyser + Cost\ of\ catalyst\ and\ membrane}{Lifetime\ of\ plant \times Mass\ of\ formic\ acid\ produced}$$

4. Operation costs

This is assumed to be 10 % of the capital costs.

$$Operation\ costs = Capital\ costs \times 10\%$$

5. Maintenance costs

This is assumed to be 10 % of the capital costs.

$$Maintenance\ costs = Capital\ costs \times 10\%$$

6. Balance of plant

The balance of plant is calculated as follows, with a balance of plant factor of 20 %.

$$Balamce\ of\ plant = Capital\ cost \times 20\%$$

7. Installation costs

$$Installation\ costs = Capital\ cost \times Lang\ factor$$

8. Cost of input chemicals

$$Cost\ of\ input\ chemicals = \frac{Cost\ of\ CO_2 \times Mass\ of\ CO_2\ converted + Cost\ of\ HMF \times Mass\ of\ HMF\ needed}{Mass\ of\ formic\ acid\ produced}$$

9. The plant-gate levelized cost can be calculated by adding up all the above costs:

$$\begin{aligned} Total\ costs \\ = Electricity\ costs + Separation\ costs + Capital\ costs + Operation\ costs + Main \\ + Balance\ of\ plant + Installation\ costs + Cost\ of\ input\ chemicals \end{aligned}$$

10. Potential profit

The profit per day from the cathode of eCO_2RR-HMFOR can be calculated based on the market price of formic acid.

$$Profit\ per\ tonne\ of\ formic\ acid = Market\ price\ of\ formic\ acid - Total\ costs$$

The profit per day from the anode of eCO_2RR-HMFOR can be calculated based on the market price of FDCA.

$$Profit\ from\ FDCA\ per\ tonne\ of\ formic\ acid = \frac{Market\ price\ of\ FDCA \times Mass\ of\ FDCA\ produced}{Mass\ of\ formic\ acid\ produced}$$

Therefore, total profits per tonne of formic acid:

$$Total\ profit = Profit\ per\ tonne\ of\ formic\ acid + Profit\ from\ FDCA\ per\ tonne\ of\ formic\ acid$$

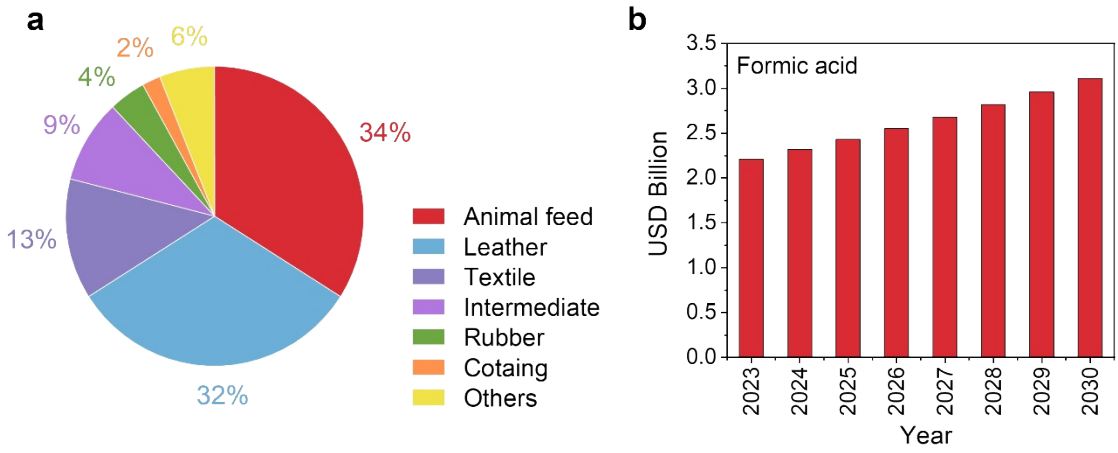
a
34%
32%
13%
9%
4%
2%
6%
Animal feed
Leather
Textile
Intermediate
Rubber
Cotaing
Others
b
Formic acid
USD Billion
3.5
3.0
2.5
2.0
1.5
1.0
0.5
0.0
2023
2024
2025
2026
2027
2028
2029
2030
Year

Figure S1. a) Application field of formic acid. The data are obtained from online, https://www.oxfa.eu/en/markets/. b) The projected market size of formic acid from 2023 to 2030. The data are obtained from Mordor Intelligence. https://www.precedenceresearch.com/formic-acid-market.

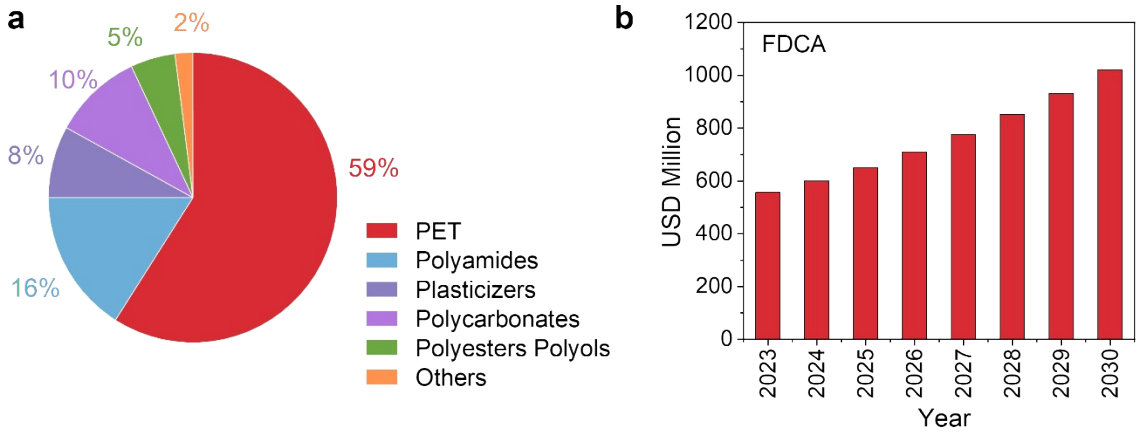

Figure S2. a) Application field of FDCA. The data are obtained from online, https://www.oxfa.eu/en/markets/. b) The projected market size of FDCA from 2023 to 2030. The data are obtained from Mordor Intelligence. https://www.acumenresearchandconsulting.com/2-5-furandicarboxylic-acid-fdca-market.

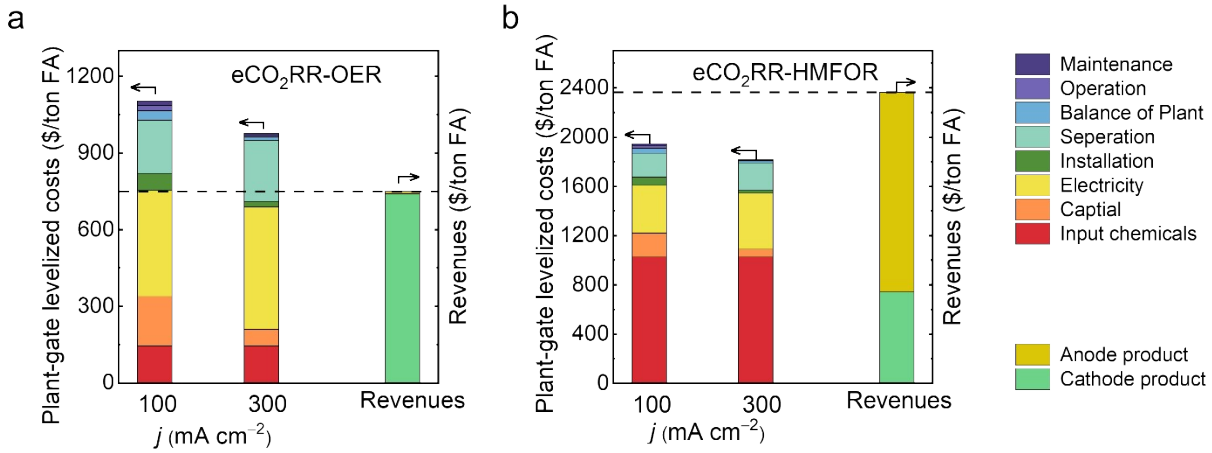

Figure S3. Techno-economic analysis of eCO_2RR-to-formate coupled (a) OER and (b) HMFOR-to-FDCA system at different current densities.

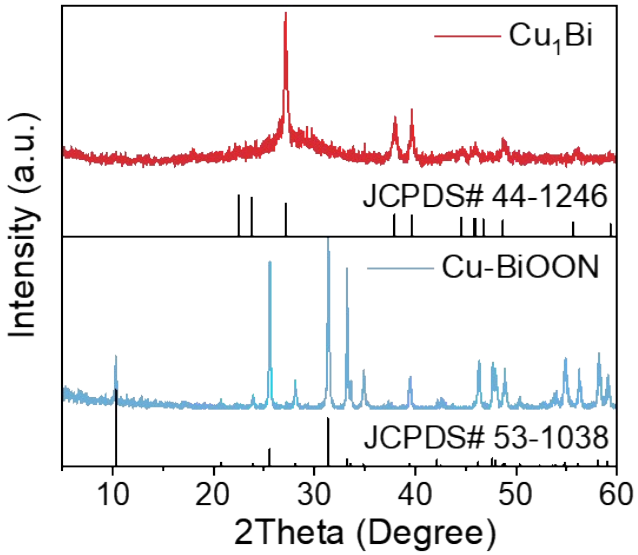

Figure S4. XRD patterns of Cu-BiOON and Cu_1Bi.

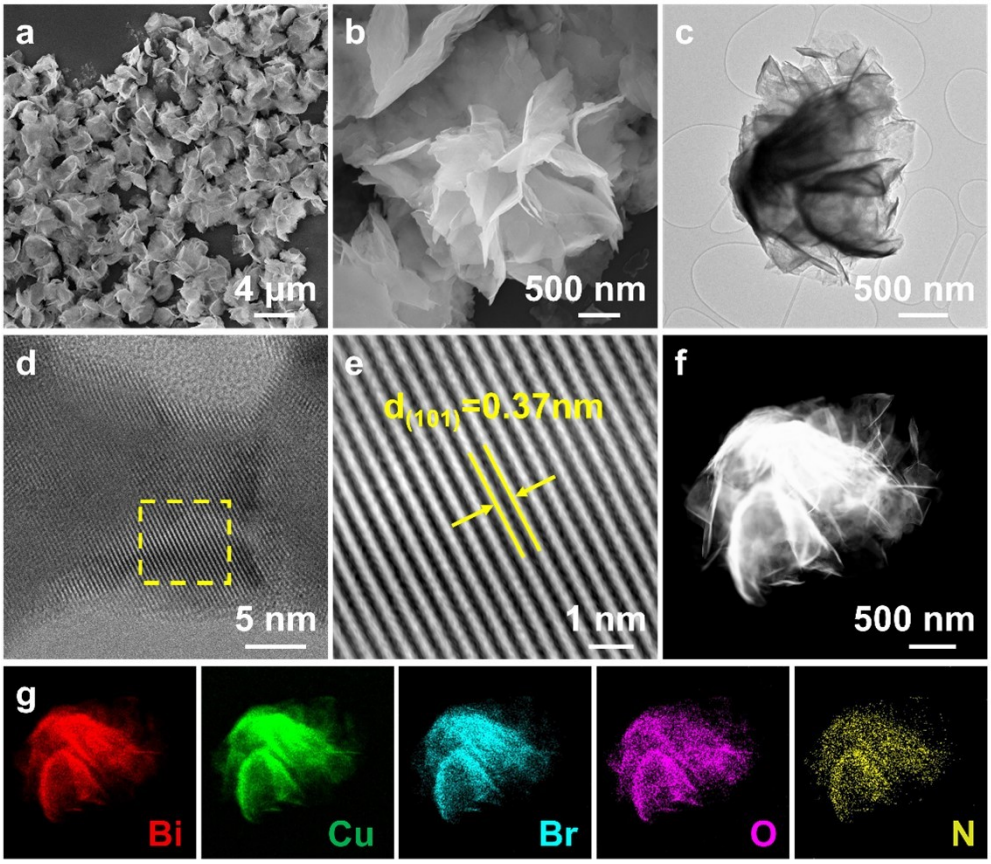

Figure S5. (a, b) SEM images, (c) TEM image, (d, e) HRTEM images, (f) STEM images and corresponding element mapping images of the as-synthesised Cu-BiOON.

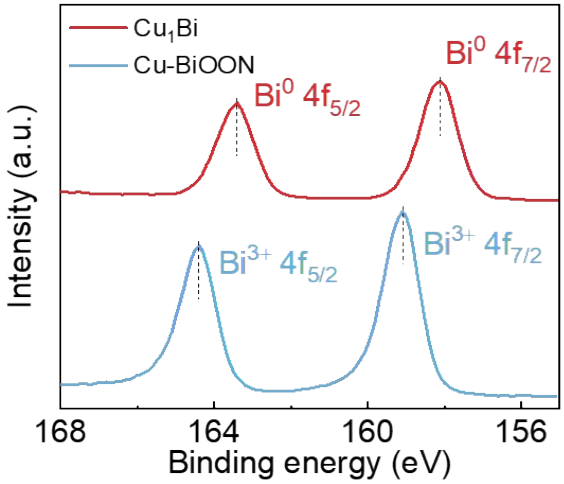

Figure S6. XPS spectra of Cu-BiOON and Cu_1Bi.

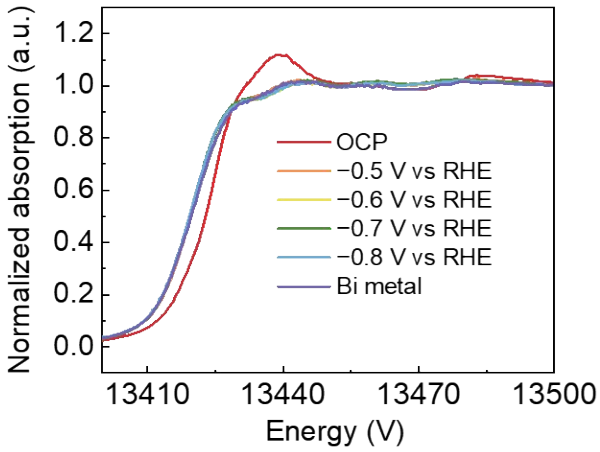

Figure S7. Bi L-edge XANES spectra acquired over Cu-BiOON electrode during eCO_2RR under open circuit potential (OCP) and different applied potentials.

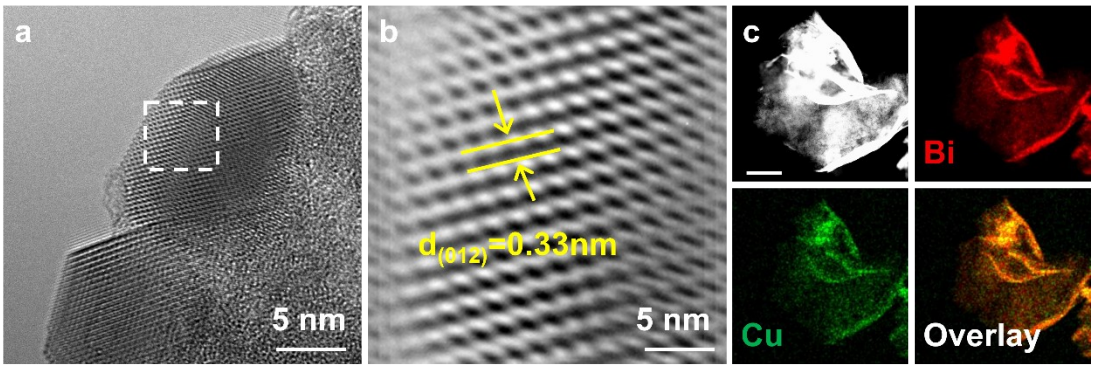

Figure S8. (a, b) HRTEM images of Cu_1Bi. c) STEM-EDS elemental mapping of Cu_1Bi. Scale bar in Figure c is 400 nm.

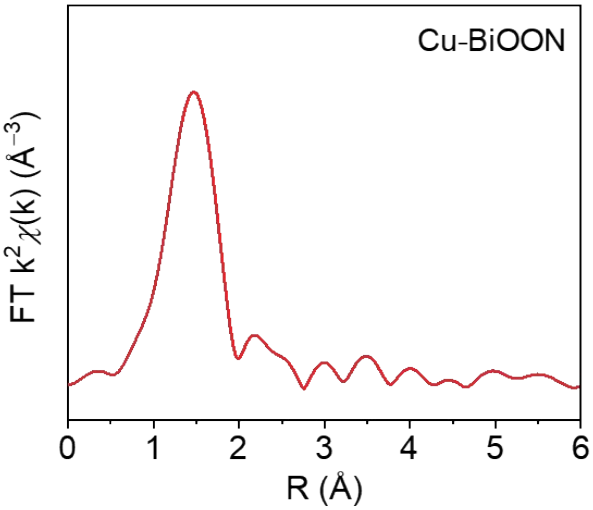

Figure S9. Cu K-edge EXAFS spectrum of Cu-BiOON.

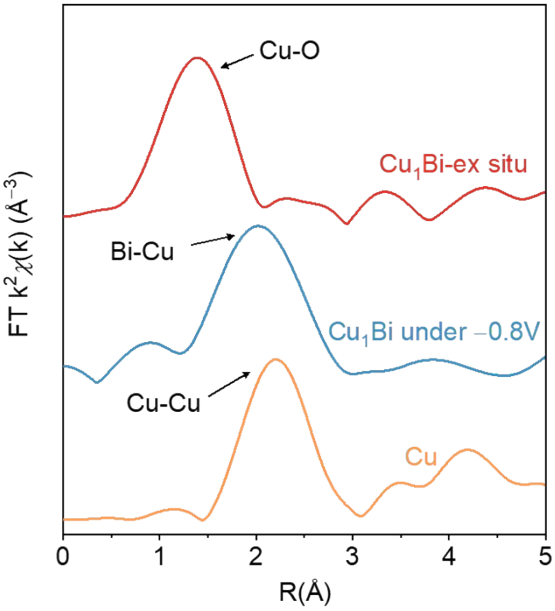

Figure S10. Cu K-edge EXAFS spectra of Cu_1Bi under ex-situ and –0.8V condition.

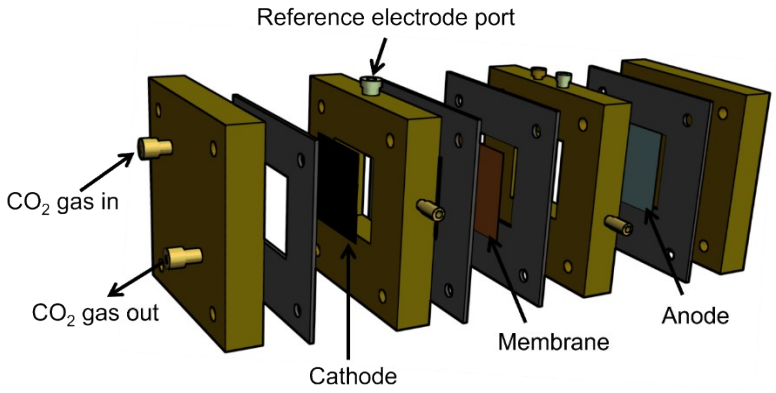

Figure S11. Expanded diagram of the flow cell.

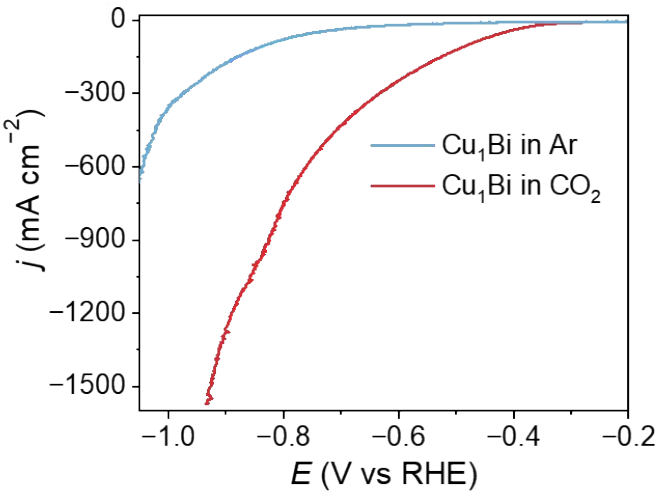

Figure S12. LSV of Cu_1Bi under Ar and CO_2 flow.

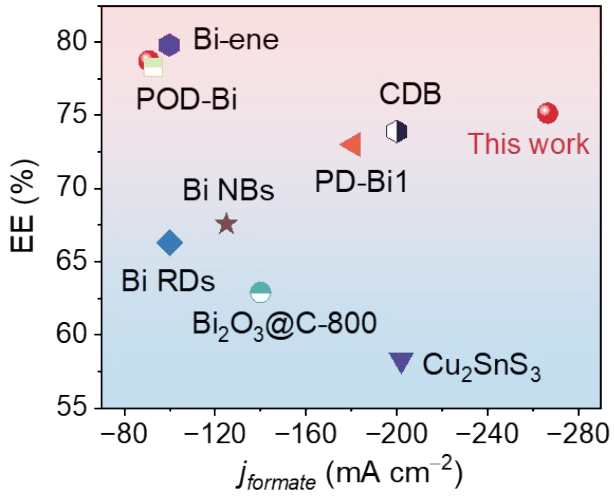

Figure S13. Comparison of energy efficiencies (EE) with recently reported formate-producing electrocatalysts with flow cell in 1 M KOH electrolyte.

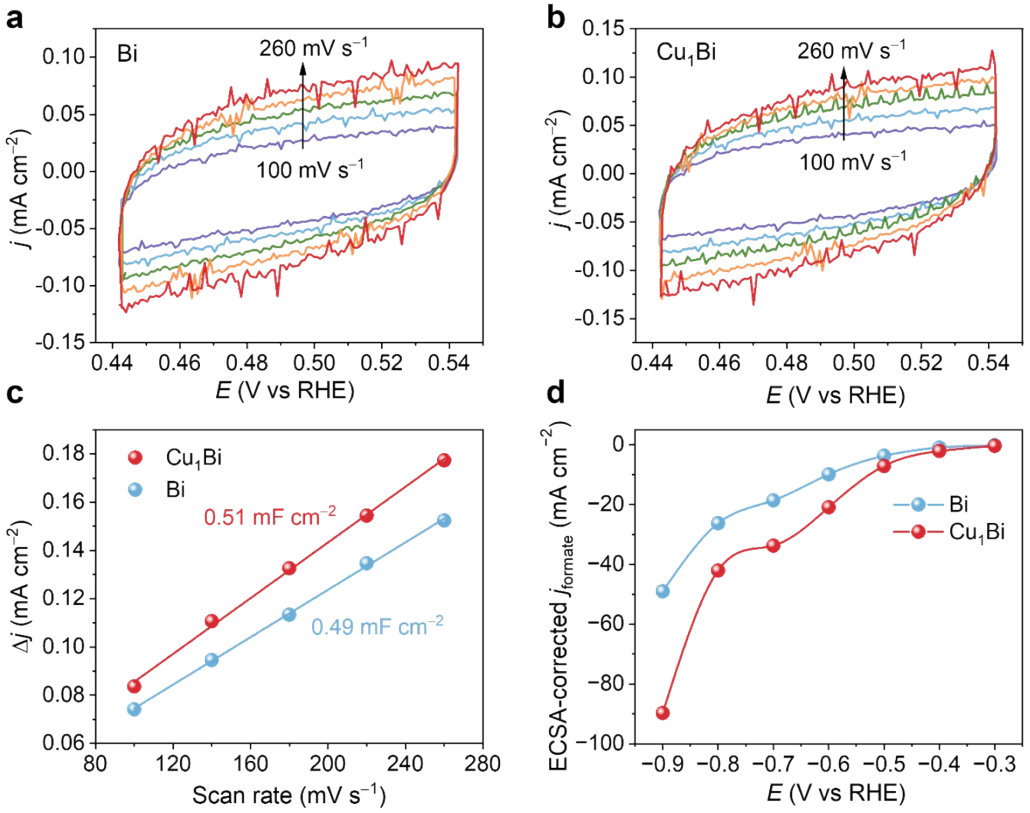

Figure S14. Cyclic voltammograms (CV) curves for (a) Bi and (b) Cu_1Bi. (c) Charging current densities differences (Δj) plotted against scan rates. (d) ECSA-corrected $j_{formate}$ of Bi and Cu_1Bi.

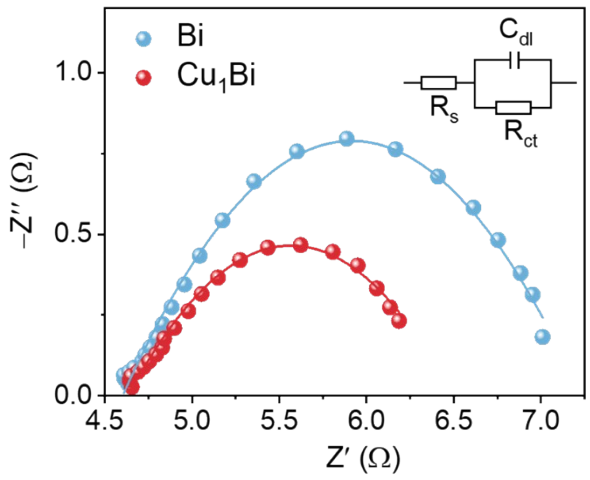

Figure S15. The fitting curves of Nyquist plots of Bi and Cu_1Bi.

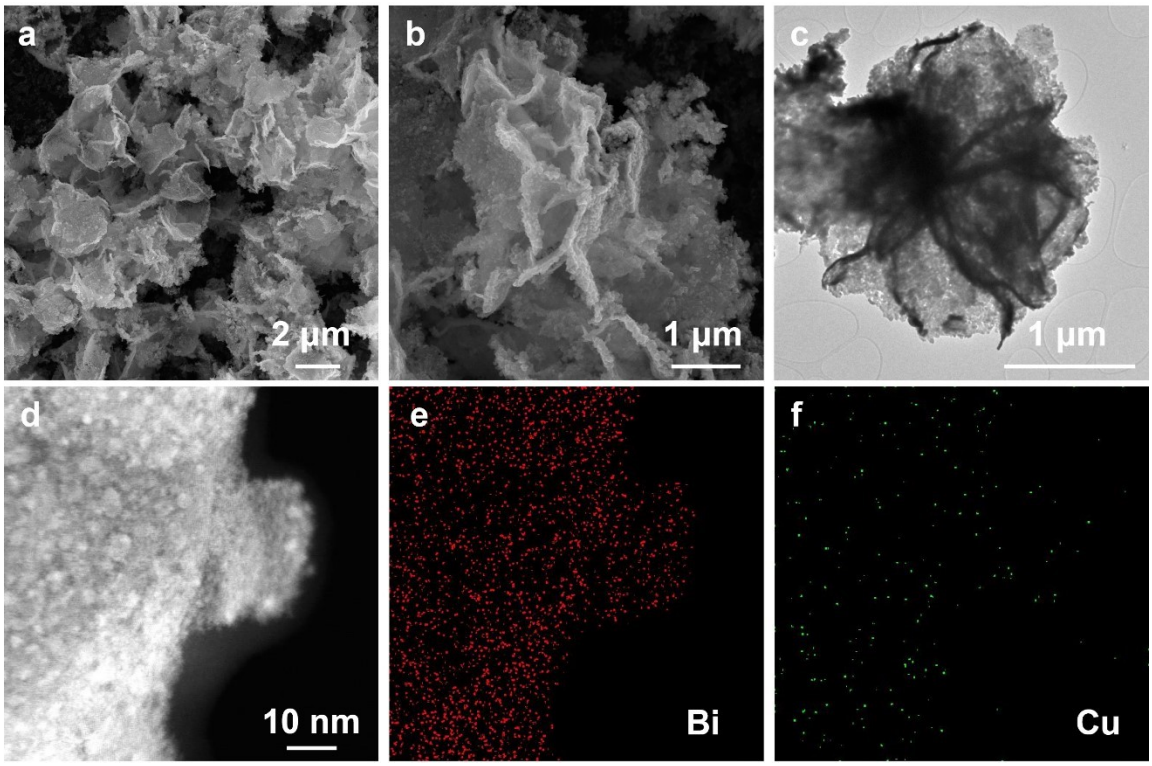

Figure S16. (a, b) SEM and (c) TEM images of Cu_1Bi post-stability electrolysis. (d) HAADF-STEM image and (e, f) corresponding element mappings of Cu_1Bi.

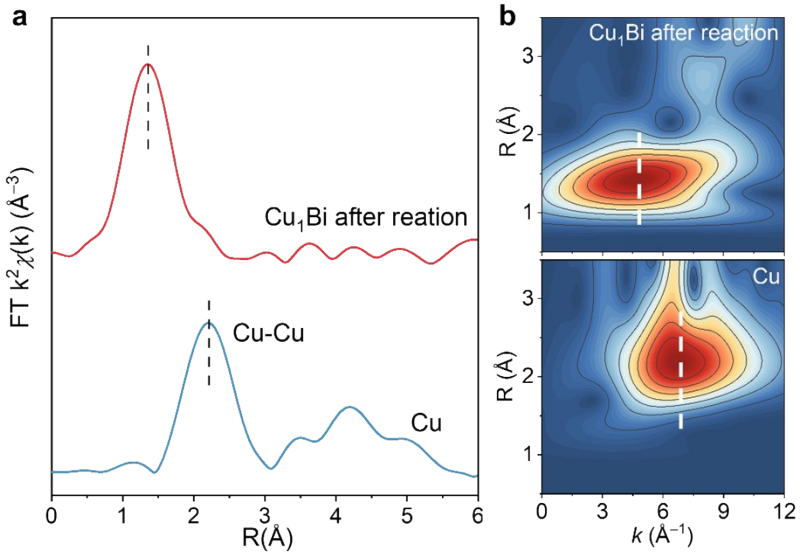

Figure S17. EXAFS spectra of Cu_1Bi post-stability test and reference Cu foil. f) WT k^2-weighted EAFS contour plots of Cu_1Bi post-stability test and reference Cu foil.

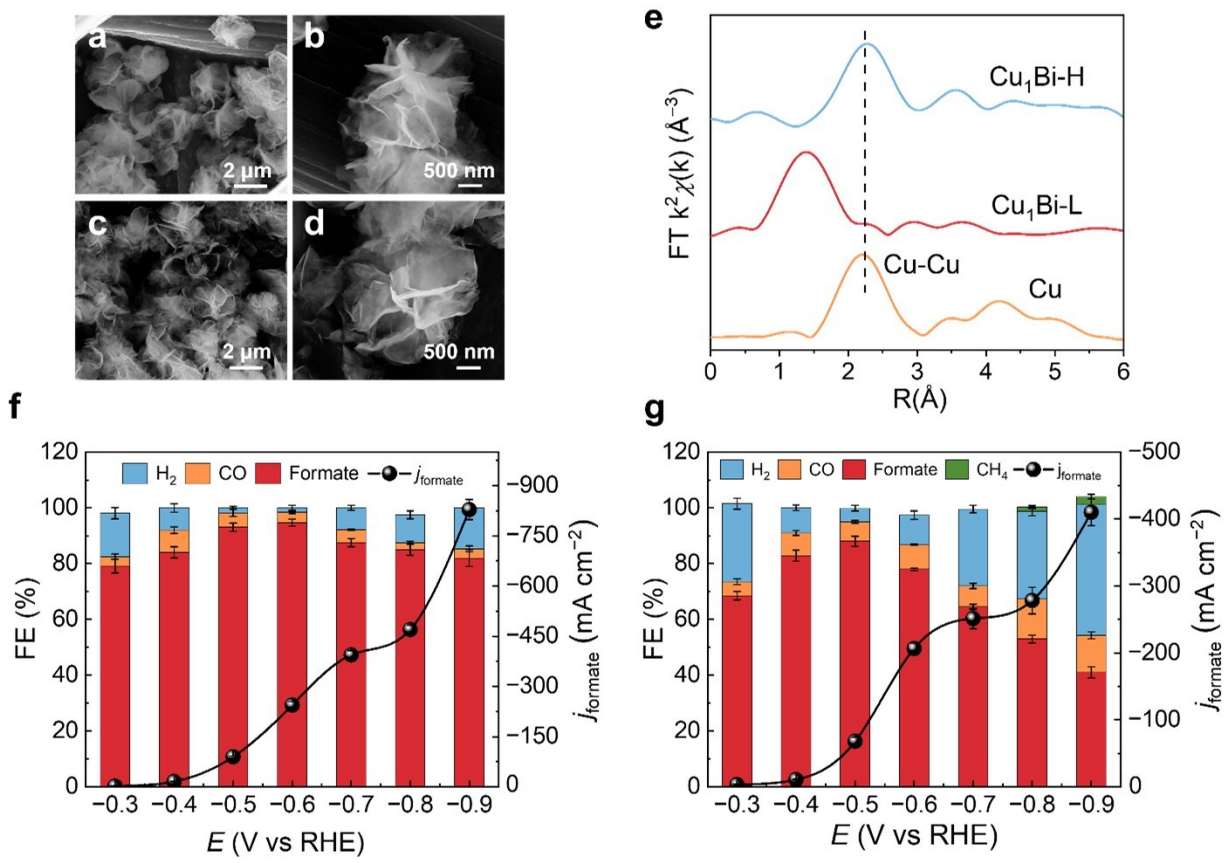

Figure S18. SEM images for (a, b) Cu_1Bi-L and (c, d) Cu_1Bi-H. (e) EXAFS spectra of Cu_1Bi-L, Cu_1Bi-H, and reference Cu foil. FEs of all the products along with the $j_{formate}$ over (f) Cu_1Bi-L and (g) Cu_1Bi-H.

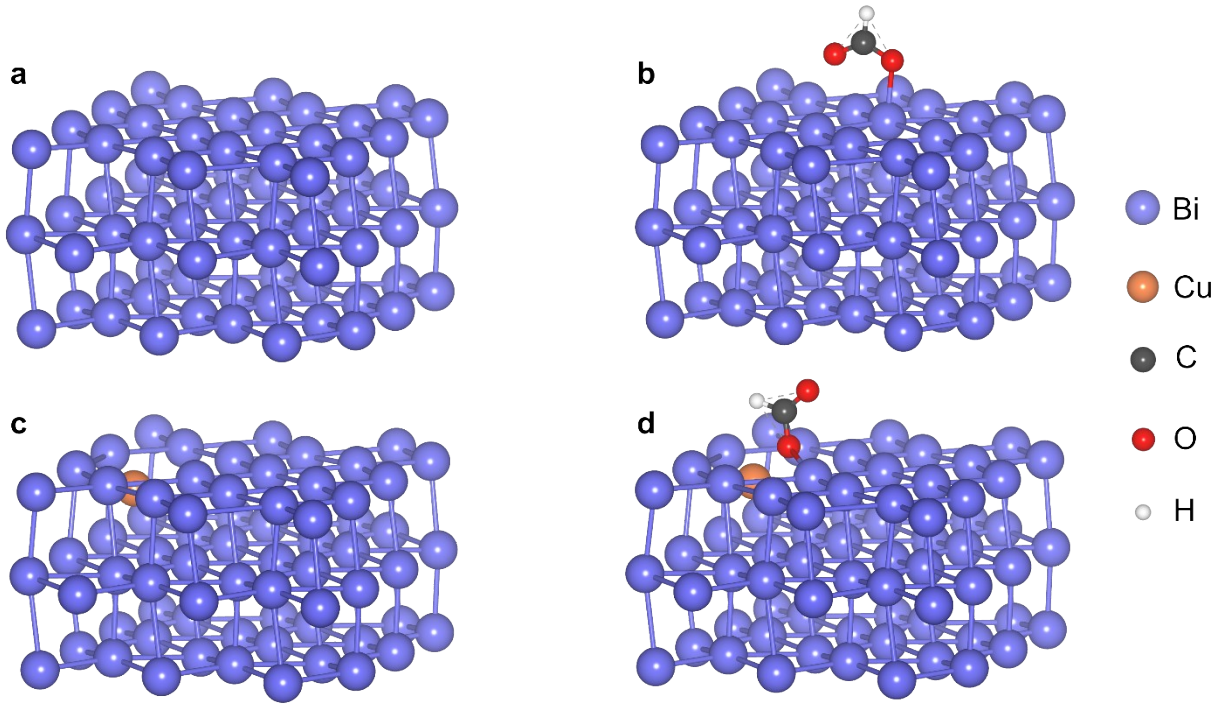

Figure S19. (a) Optimized slab model of Bi and adsorption configurations of *OCHO on (b) Bi. (c) Optimized slab model of Cu_1Bi and adsorption configurations of *OCHO on (d) Cu_1Bi.

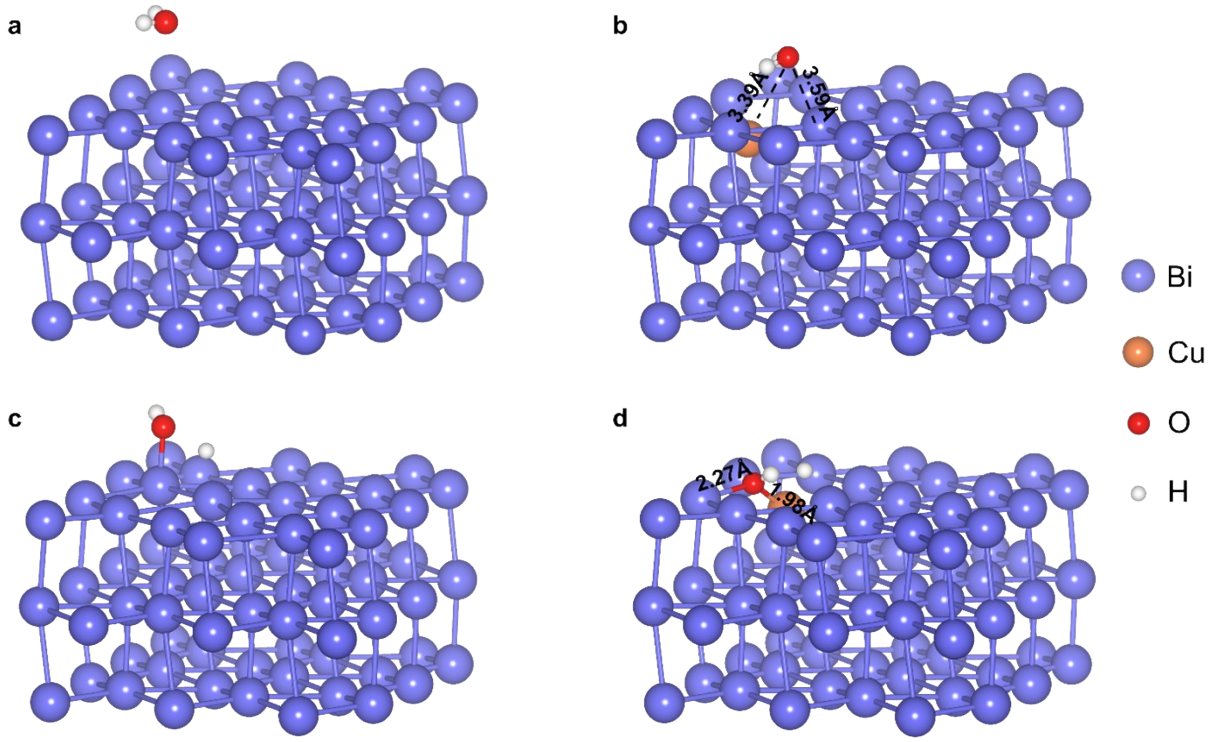

Figure S20. Optimized adsorption configurations of H_2O* on (a) Bi and (b) Cu_1Bi. Optimized co-adsorption configurations of *OH and *H on (c) Bi and (d) Cu_1Bi.

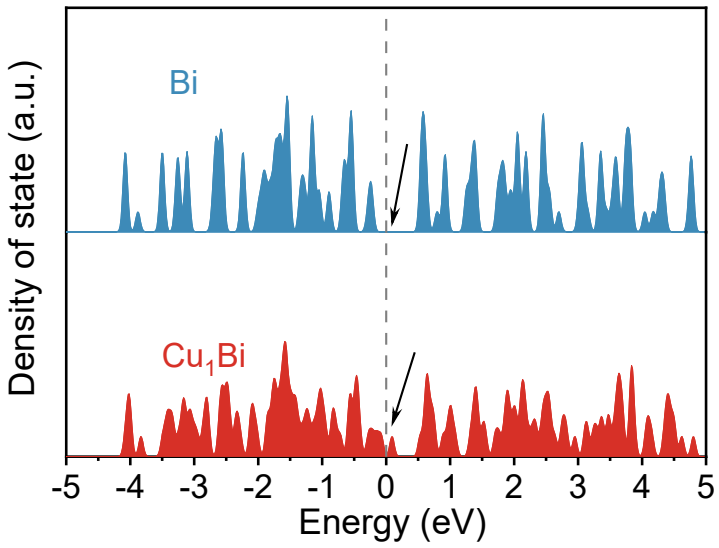

Figure S21. Density of states of Bi and Cu_1Bi.

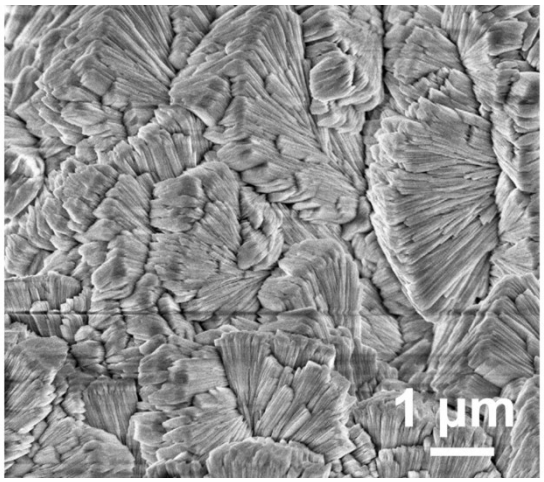

Figure S22. SEM image NiCoMOF/NF.

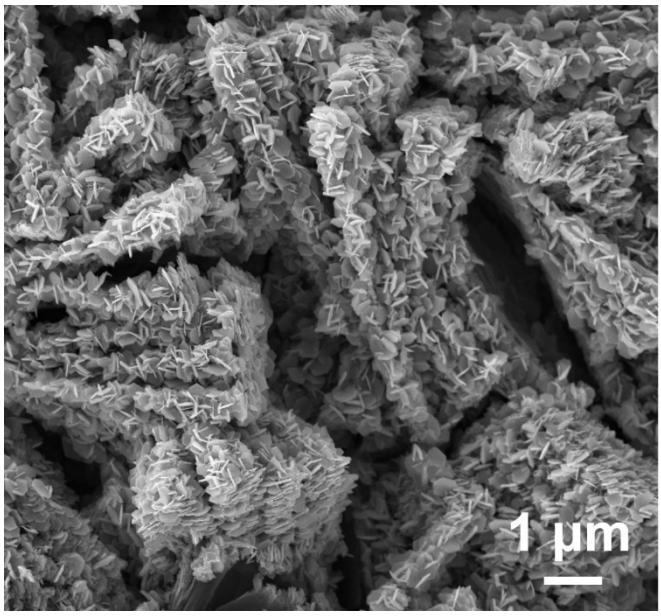

Figure S23. SEM image of NiCoLDH.

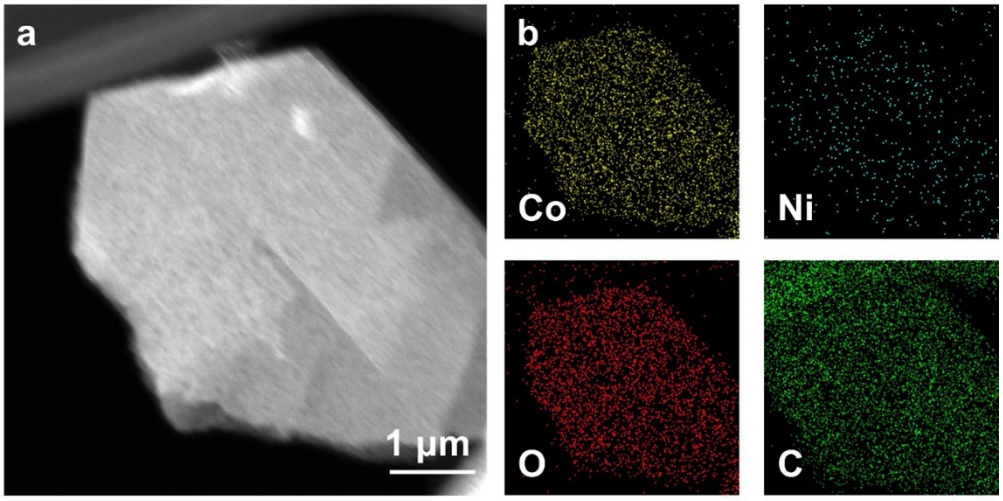

Figure S24. STEM-EDS elemental mapping of NiCoLDH.

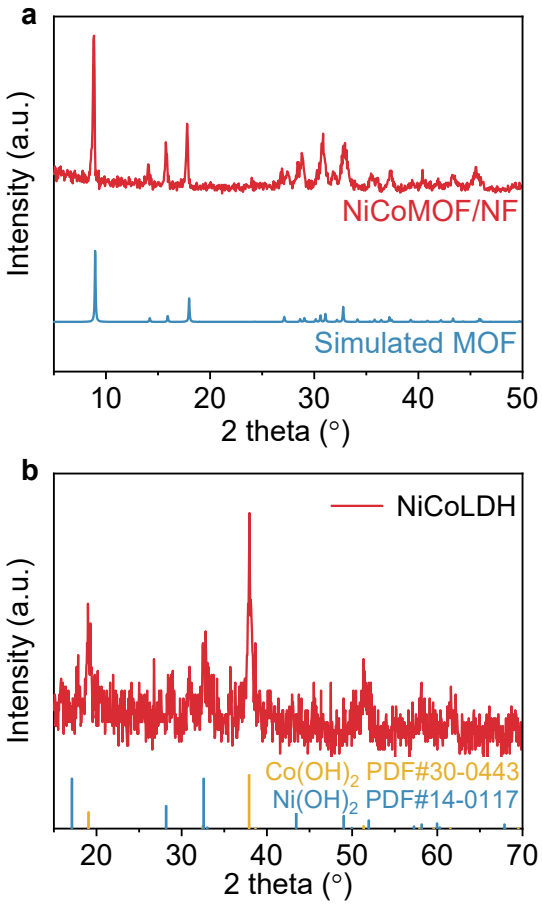

Figure S25. XRD pattern of (a) NiCoMOF and (b) NiCoLDH.

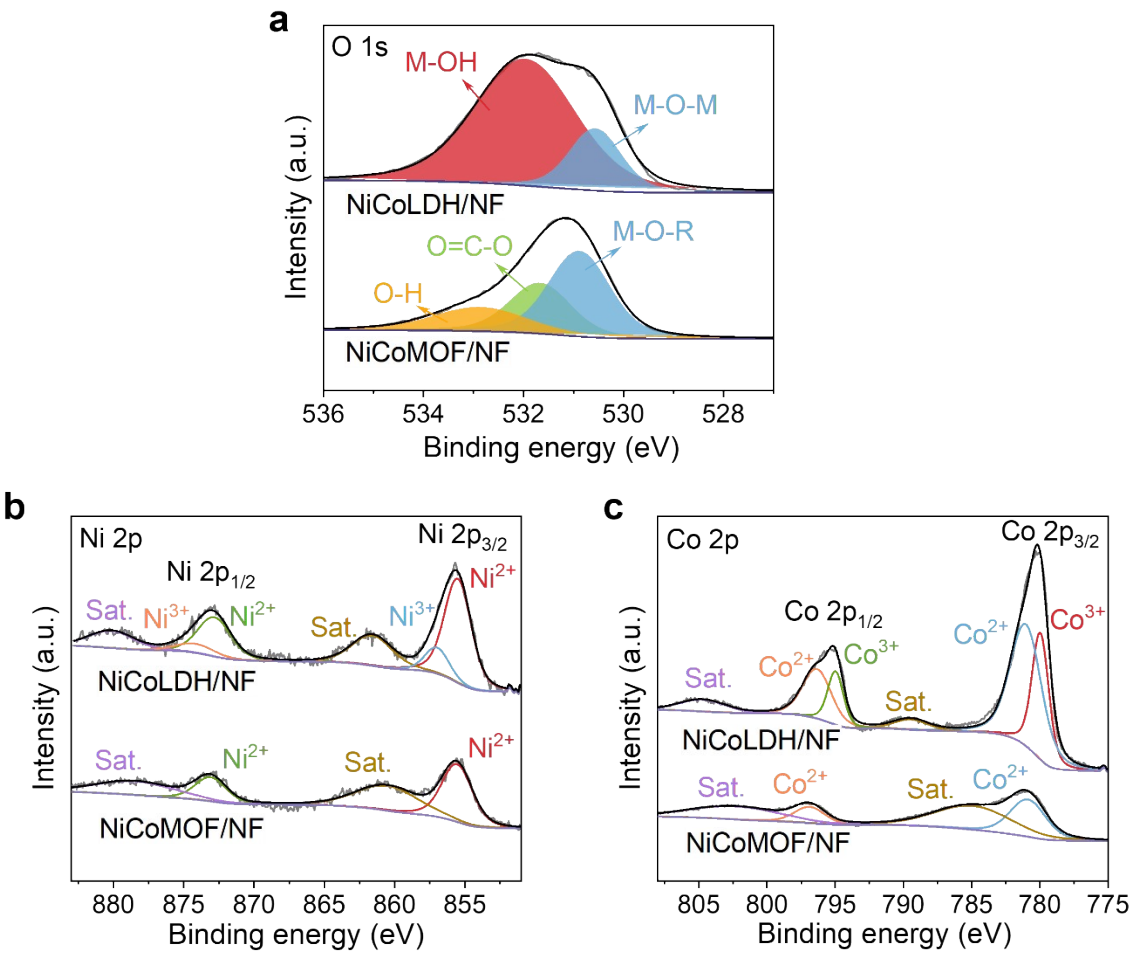

Figure S26. High resolution O 1s, Ni 2p and Co 2p XPS spectra of NiCoMOF/NF and NiCoLDH/NF.

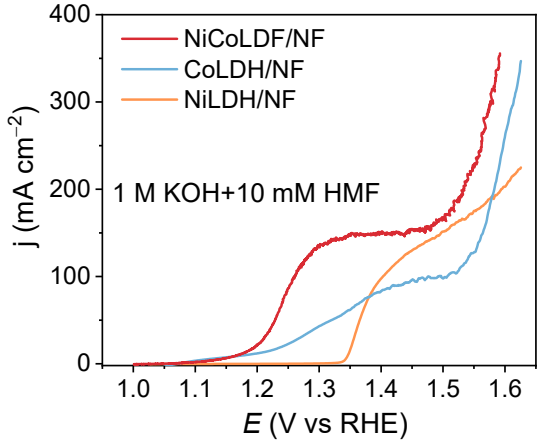

Figure S27. LSV curves of NiCoLDH/NF, CoLDH/NF, and NiLDH/NF in 1 M KOH with and without 10 mM HMF.

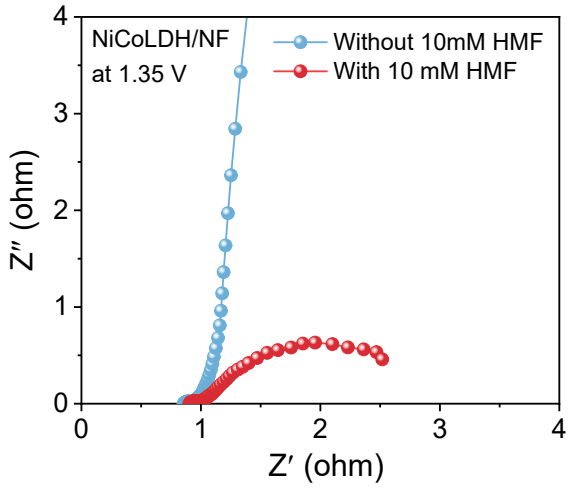

Figure S28. Nyquist plots of NiCoLDH/NF in 1 m KOH with and without 10 mM HMF at 1.35 V.

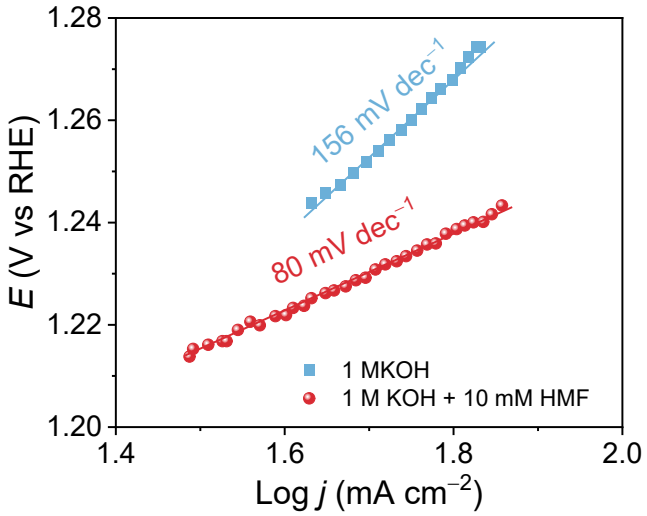

Figure S29. Tafel plots for the anodic partial HMFOR and OER derived from the LSV curves.

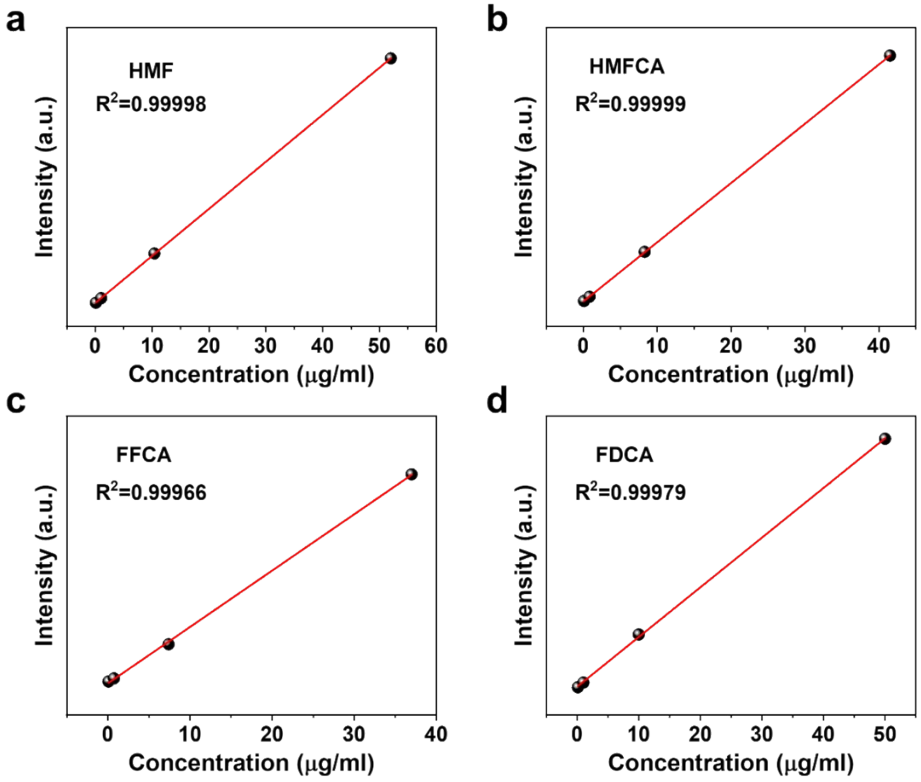

Figure S30. Calibration curves for HMF, HMFCA, FFCA, and FDCA.

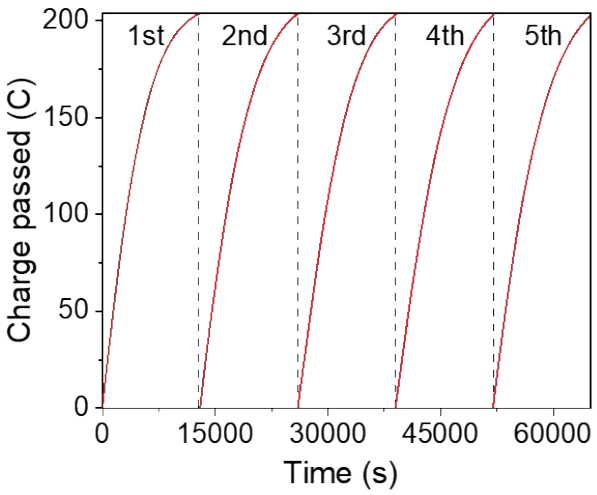

Figure S31. Charge-time curves in five successive runs.

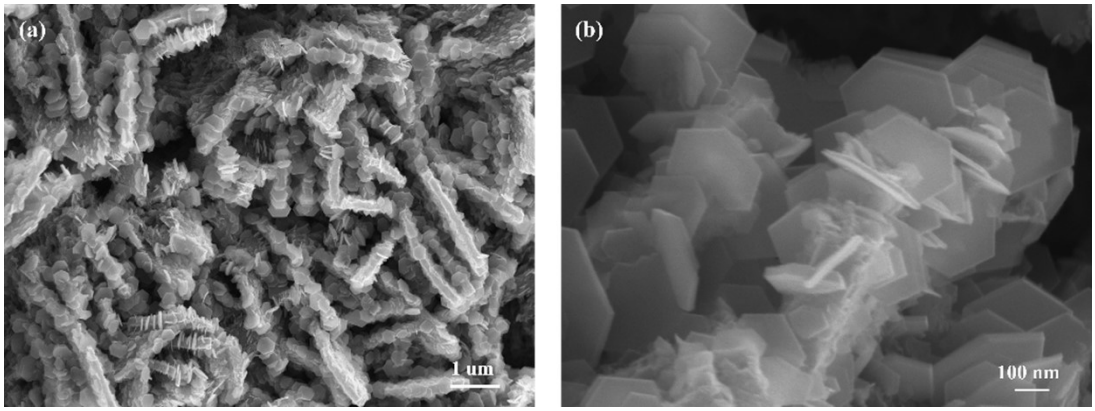

Figure S32. SEM imges of NiCoLDH after the stability measurement.

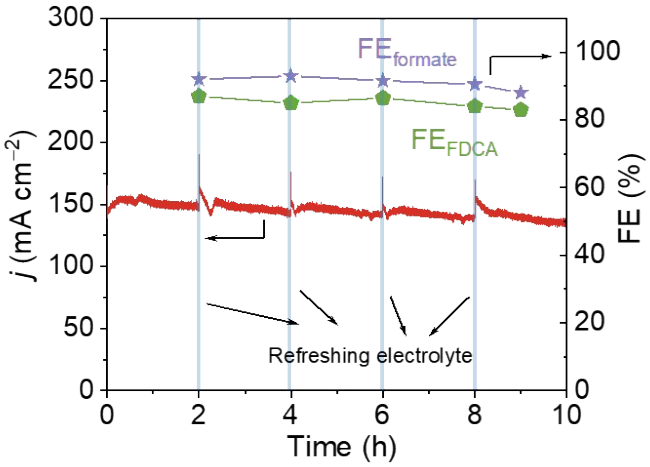

Figure S33. 10-hour stability test of eCO_2RR-HMFOR coupled system at the cell voltage of 2.35V.

Table S1. The considered parameters for techno-economic analysis.

Coupling system	j (mA cm^{-2})	Cell voltage (V)	FE_{anode} (%)	$FE_{cantode}$ (%)
eCO_2RR-OER	100	3.2	100	90
	300	3.7		
eCO_2RR-HMFOR	100	3	85	90
	300	3.5		

Table S2. Copper contents in different catalysts measured by ICP-OES.

Sample	**Cu content (wt.%)**
Cu_1Bi	1.02
Cu_1Bi-L	0.64
Cu_1Bi-H	2.82

Table S3. Comparison of eCO_2RR-to-formace performances of Bi-based and Cu-based catalysts in flow cell.

Catalyst	Electrolyte	Potential (V vs RHE)	$j_{formate}$ (mA cm^{-2})	$FE_{formate}$ (%)	Formate production rate (mmol h^{-1} cm^{-2})	Ref.
Bi_2O_3 nanotubes	1.0 M KOH	–0.61	288	98	5.38	9
Pits-Bi-NS	1.0 M KOH	–1.4	325	96	6.07	10
Bi RDs	1.0 M KOH	–0.78	290	94	5.41	11
Bi-NBs	1.0 M KOH	–1.47	331	94	6.18	12
CDB	1.0 M KOH	–0.86	600	90	11.2	13
Bi-ene-NW	1.0 M KOH	–0.97	570	-	10.64	14
BiNN-CFs	1.0 M KOH	–1.3	400	93	7.46	15
Bi_2S_3-derived	1.0 M KOH	–0.95	1860	93	35	16
BBS	1.0 M KOH	–1.25	290	83	5.41	17
nBuLi-Bi	1.0 M KOH	–1.05	410	82	7.65	18
s-SnLi	1.0 M KOH	–1.2	1100	90	18.5	19
Bimetallic Cu-Bi	1.0 M KOH	–1.0	200	92	3.74	20
Cu_2SnS_3	1.0 M KOH	–1.1	202	90	3.77	21
Cu_1Bi	1.0 M KOH	–0.7	430	94	8.03	This work
		–0.8	536	92	10.01	
		–0.9	1143	84	21.35	

Table S4. Price of feedstocks and products.

Product	Price ($/ton)	Source
Feedstocks		
CO_2	40	22
Methanol	580	23
HMF	1030	24
Products		
Formic acid	740	25
FDCA	1520	26

References

1. G. Kresse and J. Furthmüller, *Comput. Mater. Sci.*, 1996, **6**, 15-50.
2. G. Kresse and J. Furthmüller, *Phys. Rev. B*, 1996, **54**, 11169.
3. J. P. Perdew, K. Burke and M. Ernzerhof, *Phys. Rev. Lett.*, 1996, **77**, 3865.
4. G. Kresse and D. Joubert, *Phys. Rev. B*, 1999, **59**, 1758.
5. P. E. Blöchl, *Phys. Rev. B*, 1994, **50**, 17953.
6. S. Grimme, J. Antony, S. Ehrlich and H. Krieg, *J. Chem. Phys.*, 2010, **132**, 154104.
7. W. R. Leow, Y. Lum, A. Ozden, Y. Wang, D.-H. Nam, B. Chen, J. Wicks, T.-T. Zhuang, F. Li and D. Sinton, *Science*, 2020, **368**, 1228-1233.
8. P. De Luna, C. Hahn, D. Higgins, S. A. Jaffer, T. F. Jaramillo and E. H. Sargent, *Science*, 2019, **364**, eaav3506.
9. Q. Gong, P. Ding, M. Xu, X. Zhu, M. Wang, J. Deng, Q. Ma, N. Han, Y. Zhu and J. Lu, *Nat. Commun.*, 2019, **10**, 2807.
10. Y. Yuan, Q. Wang, Y. Qiao, X. Chen, Z. Yang, W. Lai, T. Chen, G. Zhang, H. Duan and M. Liu, *Adv. Energy Mater.*, 2022, **12**, 2200970.
11. H. Xie, T. Zhang, R. Xie, Z. Hou, X. Ji, Y. Pang, S. Chen, M. M. Titirici, H. Weng and G. Chai, *Adv. Mater.*, 2021, **33**, 2008373.
12. G. Zeng, Y. He, D. D. Ma, S. Luo, S. Zhou, C. Cao, X. Li, X. T. Wu, H. G. Liao and Q. L. Zhu, *Adv. Funct. Mater.*, 2022, **32**, 2201125.
13. H. Shen, Y. Zhao, L. Zhang, Y. He, S. Yang, T. Wang, Y. Cao, Y. Guo, Q. Zhang and H. Zhang, *Adv. Energy Mater.*, 2023, **13**, 2202818.
14. M. Zhang, W. Wei, S. Zhou, D.-D. Ma, A. Cao, X.-T. Wu and Q.-L. Zhu, *Energy Environ. Sci.*, 2021, **14**, 4998-5008.
15. B. Wulan, L. Zhao, D. Tan, X. Cao, J. Ma and J. Zhang, *Adv. Energy Mater.*, 2022, **12**, 2103960.
16. L. Lin, X. He, X. G. Zhang, W. Ma, B. Zhang, D. Wei, S. Xie, Q. Zhang, X. Yi and Y. Wang, *Angew. Chem. Int. Ed.*, 2023, **62**, e202214959.
17. L. Lv, R. Lu, J. Zhu, R. Yu, W. Zhang, E. Cui, X. Chen, Y. Dai, L. Cui and J. Li, *Angew. Chem. Int. Ed.*, 2023, e202303117.
18. L. Fan, C. Xia, P. Zhu, Y. Lu and H. Wang, *Nat. Commun.*, 2020, **11**, 3633.
19. S. Yan, C. Peng, C. Yang, Y. Chen, J. Zhang, A. Guan, X. Lv, H. Wang, Z. Wang and T. K. Sham, *Angew. Chem. Int. Ed.*, 2021, **60**, 25741-25745.
20. Z. Li, B. Sun, D. Xiao, Z. Wang, Y. Liu, Z. Zheng, P. Wang, Y. Dai, H. Cheng and B. Huang, *Angew. Chem. Int. Ed.*, 2023, **62**, e202217569.
21. W. Wang, Z. Wang, R. Yang, J. Duan, Y. Liu, A. Nie, H. Li, B. Y. Xia and T. Zhai, *Angew. Chem. Int. Ed.*, 2021, **60**, 22940-22947.
22. H. Shin, K. U. Hansen and F. Jiao, *Nat. Sustain.*, 2021, **4**, 911-919.
23. M. Jouny, W. Luc and F. Jiao, *Ind. Eng. Chem. Res.*, 2018, **57**, 2165-2177.
24. F. K. Kazi, A. D. Patel, J. C. Serrano-Ruiz, J. A. Dumesic and R. P. Anex, *Chem. Eng. J.*, 2011, **169**, 329-338.
25. M. Rumayor, A. Dominguez-Ramos, P. Perez and A. Irabien, *J. CO_2 Util.*, 2019, **34**, 490-499.
26. H. Kim, J. Choi, J. Park and W. Won, *Green Chem.*, 2020, **22**, 7070-7079.